Gradu Amaierako Lana/Trabajo Fin de Grado

Elektronikako Gradua/Grado en Electrónica

Microwave Photodetection with Superconducting Circuits

Borja Ramón Gómez

Director:
Prof. Iñigo L. Egusquiza
Codirector:
Dr. Mikel Sanz

Universidad del País Vasco · Euskal Herriko Unibertsitatea

FACULTY OF SCIENCE AND TECHNOLOGY
UNIVERSITY OF THE BASQUE COUNTRY

Department of Theoretical Physics and History of Science
Faculty of Science and Technology
University of the Basque Country UPV/EHU

Leioa, July 2019

Contents

Introduction and Objectives

In our day-to-day we are surrounded by processes in which detectors play a fundamental role. We do not need to think on complex activities such as industrial automatization, but on something as simple as turning on the television employing a remote control. They would be impossible to perform without these kind of devices.

The requirement of more precise and sensitive measuring devices has led to the design of detectors employing quantum resources. These devices could completely change the way we understand the world, triggering great developments in multiple disciplines. For instance, the detection of early signs of diseases, the early prediction of earthquakes, and a deeper understanding of the fundamental laws of nature could be some of the consequences to which this technology could lead.

A paradigmatic example of these devices are photodetectors, which are able to resolve single photons. Highly efficient photodetectors are essential in cutting-edge and innovative fields such as optical quantum computation, quantum communication and quantum cryptography, among others. These detectors have been developed specially for the optical frequency range. However, novel applications related to the development of quantum technologies based on superconducting platforms, such as quantum computing or quantum radars, have stimulated the interest (and necessity) of photodetection in the microwave regime, where strong efforts have been performed. This work will focus in understanding some of the proposals of flying single-photon photodetectors in the 1-10 GHz regime.

The main theoretical proposals are based on detecting a transition generated by the energy of the arriving photon emulating the photocurrent generated by the n-p photodetectors in the optical regime. Therefore, we need a physical two-level system with an energy gap similar to the energy of the photon. This kind of systems are available thanks to superconducting circuits, which are introduced in Chapter 1. After describing the linear circuit elements and their dynamics, we characterize the non-linear ones, based on the so-called Josephson junctions, an isolator sandwiched by superconducting material.

Once we have described the theoretical aspects of superconducting elements, in Chapter 2, we introduce superconducting qubits, constructed mak-

ing use of Josephson junctions, and analyse three simple but paradigmatic examples. Afterwards, we present the field of circuit quantum electrodynamics (cQED), which describes the interaction between superconducting qubits and a transmission line resonator.

Finally, in Chapter 3, we describe the problems associated to the creation of a working and efficient microwave photodetector, and analyse in depth a theoretical proposal for this device introduced in Ref. [12]. This proposal, developed in 2010, is the continuation of a previous work (Ref. [1]), which proposes a setup consisting of an infinite transmission line with a phase qubit in it. The performance achieved was of 50% efficiency employing one qubit, which could be improved by placing multiple qubits one after the other. The proposal we analyse adds a mirror to the previous setup, creating a semi-infinite transmission line. As we will see, this simple change has enormous consequences in the performance of the device.

Chapter 1

Superconducting Circuits

Superconductivity is the capacity of some materials, under certain conditions, to conduct electricity without resistance and to completely shield magnetic fields. These materials allow us to engineer superconducting circuits with intrinsic quantum behaviour, which can be controlled with external drivings.

In Section 1.1, we introduce the fundamental elements of a linear non-dissipative circuit. Then, we develop the techniques to obtain the Hamiltonian of a complete circuit to afterwards apply them to characterize the dynamics of the linear LC oscillator. To finish this Section, the transmission line and the resistor are briefly presented and analysed.

Finally, in Section 1.2, non-linear circuit elements are introduced. These elements are based on a non-linear superconducting element called Josephson junction (JJ). Using the Hamiltonian description, we analyse the Josephson LC circuit and compare it against the linear LC oscillator. Then, we present two relevant structures based on the Josephson junction, which are the DC SQUID (two JJ in parallel) and the Josephson junction array (JJ in series).

1.1 Linear Circuits

We start this Section by analysing the linear non-dissipative superconducting circuit elements, namely, linear capacitances and inductances. Then, we introduce the theoretical description of superconducting circuits. We start by presenting the canonical variables involved in a superconducting circuit, and then, we build the Hamiltonian of a circuit through the Lagrangian. Finally, we obtain the Hamiltonian of some of the most relevant linear circuits, which are the LC oscillator, the transmission line, and the resistance.

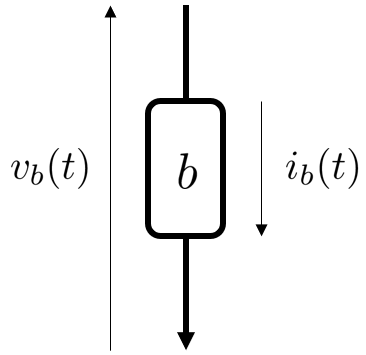

Figure 1.1: **Scheme of a branch *b* formed by a two-terminal element** and the signs of the variables of current $i_b(t)$ and voltage $v_b(t)$ associated to the branch.

1.1.1 Basic Elements

We can define an electrical circuit as a set of idealized elements connected among them in nodes, generating branches and loops, when there exist two different paths connecting two nodes. In order to mathematically analyse a circuit, we firstly need to describe the elements that form it. In this Section, among the linear non-dissipative elements, we will analyse the ones connected to two nodes, since these are the most common ones. First, we will introduce the variables that characterize the different elements and the energy of each one.

Variables of Superconducting Elements

Each branch of a circuit is characterized by two variables, namely, the current which crosses through it, $i_b(t)$, and the voltage difference, $v_b(t)$ (see Fig. 1.1). These quantities are defined by

$$v_b(t) = \int_{\text{along b}} \vec{E} \cdot \vec{dl}, \tag{1.1}$$

$$i_b(t) = \frac{1}{\mu_0} \oint_{\text{around b}} \vec{B} \cdot \vec{dS}. \tag{1.2}$$

The energy of a given branch in each instant depends on its voltage and current, and is given by

$$\varepsilon_b(t) = \int_{-\infty}^{t} v_b(t') i_b(t') dt' \tag{1.3}$$

Let us now introduce the variables of branch flux and branch charge, which are defined as

$$\phi_b(t) = \int_{-\infty}^{t} v_b(t') dt', \tag{1.4}$$

$$Q_b(t) = \int_{-\infty}^{t} i_b(t')dt'. \tag{1.5}$$

The limit $-\infty$ of the integral is due to the assumptions that the circuit was initially at rest, and that the dissipation is negligible.

We can classify the basic non-dissipative elements into two different types, depending on the relation between its variables: inductances and capacitances.

For an inductive element, the current $i_b(t)$ only depends directly on the flux $\phi_b(t)$, while for a capacitive element, the voltage $v_b(t)$ is exclusively a function of the charge $Q_b(t)$:

$$i_b(t) = f(\phi_b(t)), \tag{1.6}$$

$$v_b(t) = g(Q_b(t)). \tag{1.7}$$

Replacing these equations in the relation of the energy given by Eq. 1.3, we can obtain the energy of a branch depending on whether it is an inductive or capacitive element, which are respectively

$$\varepsilon(\phi_b) = \int_0^{\phi_b} f(\phi)d\phi, \tag{1.8}$$

$$\varepsilon(Q_b) = \int_0^{Q_b} g(Q)dQ. \tag{1.9}$$

Linear Elements

The simplest non-dissipative elements are the linear inductance and the linear capacitance, for which the relations given by Eqs. 1.6 and 1.7 are indeed linear. These relations are consequently

$$i_b(t) = \frac{\phi_b(t)}{L}, \qquad v_b(t) = \frac{Q_b(t)}{C}, \tag{1.10}$$

where L and C are the inductance and capacitance of each element respectively. Now, we can find the energy of these elements by replacing Eq. 1.10 into the expression for the energy.

In case of the linear inductance, we replace it into Eq. 1.8, and obtain

$$\varepsilon_L = \frac{\phi^2}{2L}. \tag{1.11}$$

Similarly, for the capacitance, we replace into Eq. 1.9, and get the energy of a capacitance,

$$\varepsilon_C = \frac{Q^2}{2C} = \frac{C\dot{\phi}_b^2}{2}. \tag{1.12}$$

1.1.2 Hamiltonian Description

Once the different linear non-dissipative elements of a circuit have been introduced, let us explain the theoretical description of a complete circuit. We start by presenting the variables involved in a superconducting circuit, and then, we obtain the Hamiltonian by means of the Lagrangian of the circuit.

Variables of a Circuit

First of all, we need to find the degrees of freedom of the circuit, which can be variables associated to either branches or nodes. Therefore, we have at least as much degrees of freedom as elements in the circuit. However, not all of them are true degrees of freedom, and this is due to Kirchhoff's laws, which are

$$\sum_{k=1}^{n} V_k = 0 \quad \longrightarrow \quad \sum_{\substack{\text{b around} \\ \text{loop}}} \phi_b = \tilde{\phi}_l, \tag{1.13}$$

$$\sum_{k=1}^{n} I_k = 0 \quad \longrightarrow \quad \sum_{\substack{\text{b arriving} \\ \text{at node}}} Q_b = \tilde{Q}_n, \tag{1.14}$$

where $\tilde{\phi}_l$ is the static flux through a loop and $\tilde{Q}_n$ the charge offset in a node.

We have already described the variables associated to the branches formed by linear elements (Eq. 1.10), so let us now introduce the connection between the descriptions employing branches and using nodes.

The node description is based on building a spanning tree from a particular node of our choice, which we call "ground". The spanning tree is built by connecting the rest of the nodes through branches in a way that no loop is formed. The branches which are not chosen in the spanning tree are called closure branches. We can now define the flux of a node as the sum of the fluxes of all the branches in the path between the ground and the node itself. Therefore, the flux of a branch b can be defined in terms of the flux of the nodes connected by the branch, n and n', as

$$\phi_b = \phi_n - \phi_{n'}. \tag{1.15}$$

In the case of a closure branch, the one which closes a loop l, from Eq. 1.13 we deduce that

$$\phi_b = \phi_n - \phi_{n'} - \tilde{\phi}_l. \tag{1.16}$$

Lagrange-Hamilton Formulation

To obtain the Hamiltonian, we firstly need the Lagrangian of the circuit, which is defined as the difference between the kinetic energy and the potential energy. This can be obtained by arbitrarily attributing the potential

energy to the inductances and the kinetic energy to the capacitances. Therefore, the Lagrangian is given by

$$\mathcal{L} = \sum_{\mathrm{C}} \mathcal{T}_b - \sum_{\mathrm{L}} \mathcal{U}_b, \tag{1.17}$$

where $\mathcal{T}_b$ and $\mathcal{U}_b$ are respectively the kinetic and potential energies of the branches of the circuit. Both quantities are written in terms of the flux of the branches, and its time derivative. In order to write the Hamiltonian, we need the conjugate momenta of the branch fluxes, which are defined as

$$q_b = \frac{\partial \mathcal{L}}{\partial \dot{\phi}_b}. \tag{1.18}$$

We now write the Hamiltonian $\mathcal{H}$ as the Legendre transform of the Lagrangian,

$$\mathcal{H} = \sum_b \dot{\phi}_b q_b - \mathcal{L}, \tag{1.19}$$

by replacing the $\dot{\phi}_b$ by the canonical momenta. Finally, we perform the canonical quantization replacing the classical variables by operators and imposing that the commutator is given by the usual relation

$$[\phi_b, q_b] = i\hbar. \tag{1.20}$$

1.1.3 LC Circuit

The LC oscillator is the simplest superconducting circuit comprising a linear capacitance and a linear inductance in parallel (Fig. 1.2a). In order to find its Hamiltonian, we first define the Lagrangian by replacing the energies of the elements, given by Eqs. 1.8 and 1.9, into Eq. 1.17. The results is

$$\mathcal{L} = \frac{C\dot{\phi}^2}{2} - \frac{\phi^2}{2L}, \tag{1.21}$$

$$\mathcal{H} = \frac{C\dot{\phi}^2}{2} + \frac{\phi^2}{2L} = \frac{q^2}{2C} + \frac{\phi^2}{2L}. \tag{1.22}$$

Notice that this Hamiltonian is the same as for a mechanical harmonic oscillator, $H = p^2/2m + m\omega^2 x^2/2$, where $m = C$, $\omega = 1/\sqrt{LC}$, and the operator q is equivalent to the momentum and ϕ to the position. After defining two new operators, namely, the reduced charge $n = q/2e$ and the reduced flux $\varphi = 2\pi\frac{\phi}{\phi_0}$, where e is the electron charge and $\phi_0 = h/2e$ is known as the superconducting flux quantum, the Hamiltonian can be written as

$$\mathcal{H} = 4E_C n^2 + \frac{1}{2}E_L \varphi^2, \tag{1.23}$$

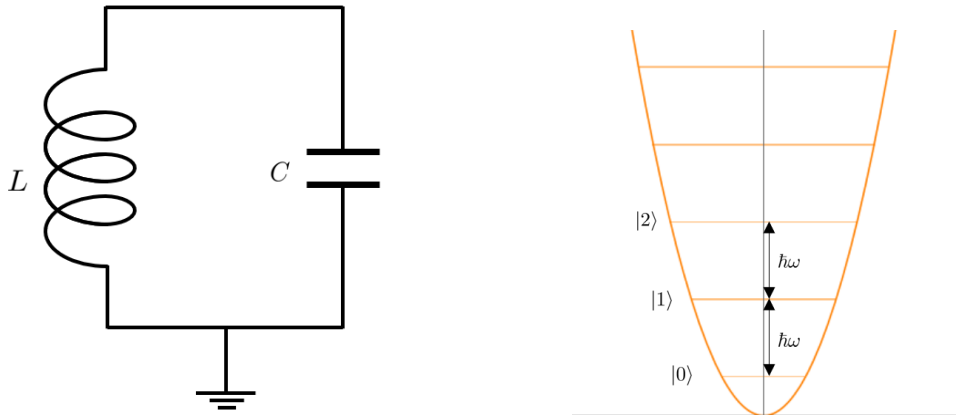

(a) (b)

Figure 1.2: **Representation of a LC oscillator (a) and its respective potential and energy levels (b).** In figure (b) is plotted the potential term of Eq. 1.23, which is a parabola. The energy levels are all equally distant, with an energy gap of $\hbar\omega$.

where $E_C = e^2/2C$ is the electrostatic energy and $E_L = \phi_0^2/(4\pi^2 L)$ is the inductive energy. In order to represent the Hamiltonian in a more compact and convenient form, we describe the operators n and φ in terms of the ladder operators (a, $a^\dagger$):

$$n = \left(\frac{E_L}{32E_C}\right)^{1/4} i(a - a^\dagger), \quad \varphi = \left(\frac{2E_C}{E_L}\right)^{1/4} (a + a^\dagger). \tag{1.24}$$

This change of operators results in [2]

$$\mathcal{H} = \hbar\omega(a^\dagger a + 1/2), \tag{1.25}$$

where the operator $a^\dagger a$ represents the number of charge units in the resonator. In the case of a superconducting circuit, this unit of charge is the Cooper pair, formed by two electrons and, therefore, with a charge $2e$.

The state of the system, $|n\rangle$, is determined by the number of Cooper pairs in the resonator. Notice that the energy levels given by this circuit, represented in 1.2b, are equispaced by a value of $\hbar\omega = \hbar/\sqrt{LC}$.

1.1.4 Transmission Line

Transmission lines are central elements in experimental superconducting circuits, since they are used to control other elements and for the read-out of information from superconducting circuits.

There is a wide variety of transmission lines, but the one used in superconducting circuits is the coplanar waveguide (CPW). It is a pretty simple structure: a superconducting line in the centre with two ground planes on

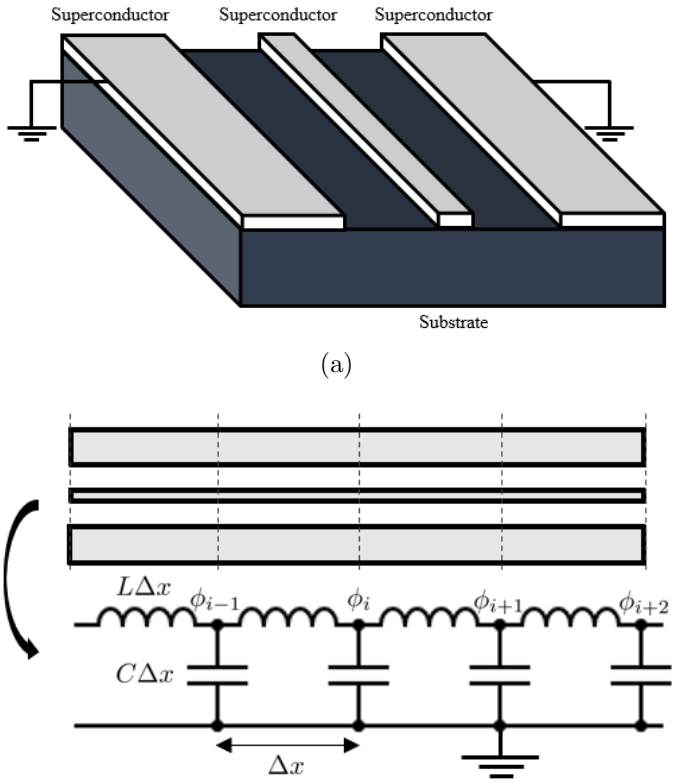

Figure 1.3: **Coplanar waveguide (CPW).** (a) Physical scheme of a CPW, made of three superconducting strips in the same plane on a substrate. The central strip carries the signal, and the lateral strips are the ground planes. (b) Theoretical model. The scheme of the bottom of the figure represents a CPW in the limit $\Delta x \to 0$. The infinite nodes are labelled with i, each with a node flux ϕ_i.

its sides, and all on top of a dielectric substrate (see Fig. 1.3a). This particular configuration is used in printed circuits and transports signals in the microwave regime [3].

We can model a coplanar waveguide as N individual Δx-wide slices connected in series in the limit $\Delta x \to 0$ (or $N \to \infty$), where $N\Delta x$ is equal to the total length of the transmission line [4]. Each individual slice can be represented as a LC circuit (see Fig. 1.3b). The capacitive element, with capacitance $C\Delta x$, represents the capacitance formed between the superconducting central line and the ground planes, and the inductive element, with inductance $L\Delta x$, represents the magnetic field produced by the current passing through the superconductor, where C and L are the density of capacitance and inductance per length unit of the transmission line.

Therefore, the Lagrangian (Eq. 1.17) of a CPW is an infinite sum over the energy of the capacitances, whose branch flux is the same as the node

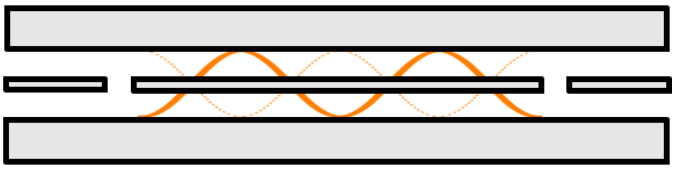

Figure 1.4: **Scheme of a coplanar waveguide resonator.** The orange lines represent a stationary mode, forming antinodes at the ends.

flux ϕ_i, and another sum over the inductances, whose branch flux is $\phi_i - \phi_{i-1}$. The Hamiltonian (Eq. 1.19) results in

$$\mathcal{H} = \lim_{\Delta x \to 0} \sum_{i=-\infty}^{\infty} \left[\frac{C\Delta x}{2} \dot{\phi}_i^2 + \frac{1}{2L\Delta x} (\phi_i - \phi_{i-1})^2 \right]. \tag{1.26}$$

Microwave Resonators

Apart from signal communication, superconducting coplanar waveguides are also used in the design of microwave resonators. In a transmission line resonator, the electric field travels confined in the space between the central and the ground planes. Two gaps in the central superconducting line, which behave as capacitances, delimit the boundaries of the resonator (see Fig. 1.4). This boundary conditions mean that the electric field has an antinode in both ends of the cavity.

1.1.5 Resistor

It is noteworthy to briefly describe the case of a paradigmatic linear dissipative element:the resistor. As the dissipation is an irreversible phenomenon, the Hamiltonian formulation is subtle. This problem is solved by considering the resistor characterized by an admittance $Y(\omega) = 1/Z(\omega)$ as an infinite set of LC circuits (see Fig. 1.5) and, afterwards, finding a master equation for the system by tracing out the LC degrees of freedom. This leads to the so-called Caldeira-Leggett model [5]. The Hamiltonian of this model results in

$$\mathcal{H} = \sum_{i=1}^{\infty} \left[\frac{C_i}{2} \dot{\phi}_i^2 + \frac{1}{2L_i} (\phi_i - \phi)^2 \right], \tag{1.27}$$

where the sum runs for every LC circuit and ϕ denotes the node flux of one of the ends of the admittance. The remaining node has been considered as the ground.

1.2 Non-Linear Circuits

In the previous Section, we have observed that the LC circuit shows quantum behaviour in the quantization of the energy levels. Let us now add

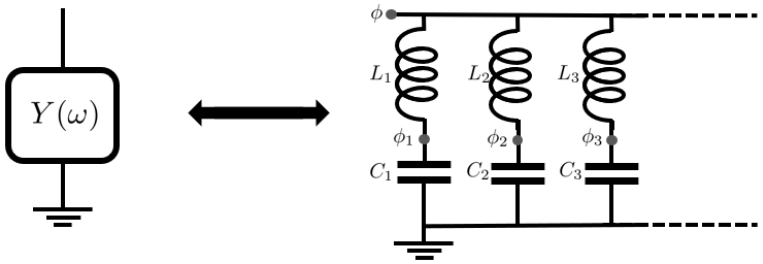

Figure 1.5: **Caldeira-Leggett model of an admittance $Y(\omega)$.** The node flux of one of its ends is ϕ, and the other one is taken as ground. Each of the infinite number of LC circuits, with capacitance C_i and inductance L_i, is characterized by the node flux ϕ_i.

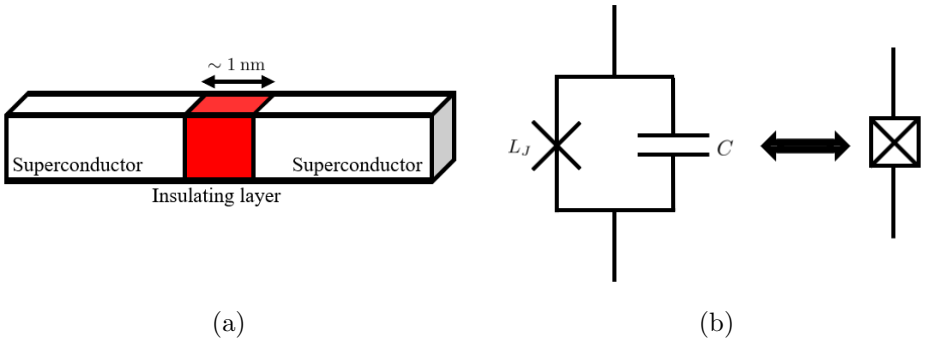

Figure 1.6: **Scheme of a Josephson junction (a) and its equivalent circuit (b)** in therms of a non-linear inductance (L_J) and a linear capacitance (C). It can also be pictured as a cross in a square.

non-linear elements into the circuits. The element at our disposal for this purpose is the Josephson junction, which consists in an isolator sandwiched by superconductors. In this Section, we describe this element and solve the Hamiltonian for the Josephson LC oscillator. Finally, we present two useful devices composed of Josephson junctions, which are the DC SQUID and the Josephson junction array.

1.2.1 Josephson Junction

The Josephson junction (JJ) is a non-linear element formed by two superconducting plates with a 1-10 nm thin insulating layer in between (see Fig. 1.6a), through which pairs of electrons, called Cooper pairs, cross due to the tunnel effect. This element is considered a cornerstone in superconducting circuits.

The pure JJ, i.e. discarding dissipative contributions, can be theoretically modelled as a non-linear inductance (Josephson element) in parallel with a linear capacitance (see Fig. 1.6b). Let us now characterize the Josephson element to obtain the energy corresponding to the whole Josephson junction. It can be obtained by replacing the two Josephson relations

in Eq. 1.8, which leads to

$$I = I_c \sin(\varphi(t)), \qquad V = \frac{\hbar}{2e}\frac{\mathrm{d}\varphi(t)}{\mathrm{d}t}, \tag{1.28}$$

with I_c the critical current, the maximum current which can cross the junction before it becomes resistive. The flux $\varphi = 2\pi\frac{\phi_J(t)}{\phi_0} = \frac{2e}{\hbar}\phi_J(t)$ is known as the reduced flux, where ϕ_J is the flux through the Josephson element and ϕ_0 is the superconducting flux quantum. Using these relations and keeping in mind that the inductance of an inductive element is $L_b = (\frac{\mathrm{d}i_b}{\mathrm{d}\phi_b})$, we find out that the inductance of a Josephson junction is clearly non-linear:

$$L_J = \frac{\phi_0}{2\pi I_c \cos\left(2\pi\frac{\phi_J}{\phi_0}\right)}. \tag{1.29}$$

Now, we use this equation to find the energy of the non-linear inductance

$$\varepsilon_J = \int_0^{\phi_J} I_c \sin\left(\frac{2\pi\phi}{\phi_0}\right) d\phi = \frac{\phi_0}{2\pi} I_c (1-\cos\left(\frac{2\pi\phi_J}{\phi_0}\right)) = E_J(1-\cos\varphi), \tag{1.30}$$

where $E_J = \phi_0 I_c/2\pi$ is the Josephson energy.

1.2.2 Josephson LC Circuit

The equal spacing between energy levels in the LC harmonic oscillator (Fig. 1.2) makes impossible to address the excitation of a specific state, since the energy required is the same. This fact limits the usefulness of the linear LC oscillator in quantum computation since we need a well defined two-level subsystem to be used as a qubit. To address this problem, we introduce the non-linear Josephson junction to replace the linear inductance (Fig. 1.7a). The new system is described by the Hamiltonian

$$\mathcal{H} = 4E_C n^2 - E_J \cos(\varphi), \tag{1.31}$$

where $E_C = e^2/2C_\Sigma$ and $C_\Sigma = C_S + C_J$ depend on both the shunt capacitance C_S and the capacitance of the junction C_J.

The potential energy is now sinusoidal instead of parabolic (Fig. 1.7b). Therefore, the energy levels are no longer equally spaced [6], which allows us to control the transitions between only two levels. This is typically performed using the ground and the first excited states, with a transition energy of $\hbar\omega_{01}$. As the excitation between two levels can be individually addressed, this circuit can be considered a qubit.

The characteristics of a qubit highly depend on which is the dominant term of the Hamiltonian. A qubit with a JJ and a linear capacitance is characterized by the ratio E_J/E_C. It is worth mentioning that the general form of a simple superconducting qubit also includes a linear inductance shunting the Josephson junction, which adds an additional term to the Hamiltonian. Then, in general, superconducting qubits are also characterized by another ratio, $\frac{E_J - E_L}{E_L}$.

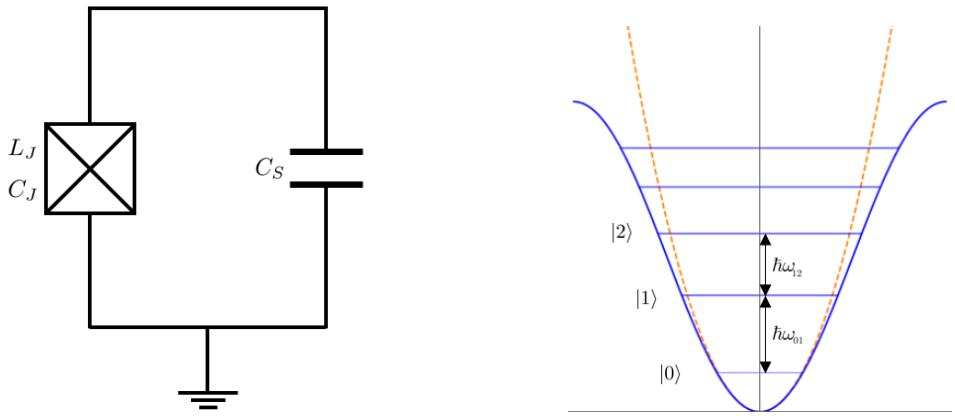

Figure 1.7: **Representation of a Josephson LC oscillator (a) and its potential energy and energy levels (b).** In figure (b) is plotted the potential term Eq. 1.31 in blue and the potential of the linear LC circuit (Eq. 1.22) with an orange dashed line. The energy gap between two levels is not constant.

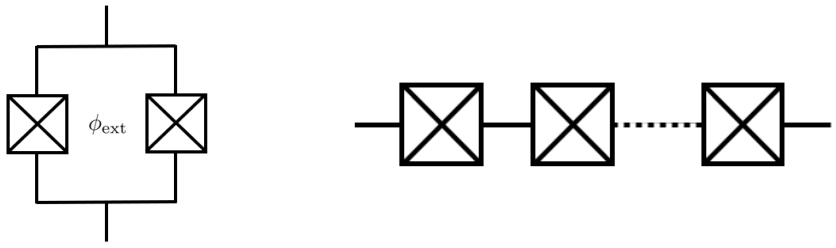

Figure 1.8: **(a) DC SQUID with an external flux ϕ_{ext} throughout the loop**, formed by two Josephson junctions in parallel. **(b) Josephson junction array**, formed by Josephson junctions in series.

1.2.3 DC SQUID

The circuit called DC SQUID (from *Superconducting Quantum Interference Device*) consists of two Josephson junctions in parallel, forming a superconducting loop (see Fig. 1.8a). We can calculate its Hamiltonian using the energy of the Josephson junction, which is composed of a Josephson element (Eq. 1.30) and a lineal capacitance (Eq. 1.9). The Hamiltonian of a DC SQUID is

$$\mathcal{H}_{\text{SQ}} = 4E_C n^2 - E_{J1}\cos(\varphi_1) - E_{J2}\cos(\varphi_2), \tag{1.32}$$

where $E_C = e^2/2C_\Sigma$, $C_\Sigma = C_{J1} + C_{J2}$ is the energy corresponding to the capacitances of the Josephson junctions, and E_{J1}, E_{J2} the energy of the Josephson elements.

For the sake of simplicity, we will consider both Josephson junctions identical ($E_{J1} = E_{J2} = E_J$). Employing Eq. 1.13, we can relate the fluxes

of each junction as $\varphi_1 - \varphi_2 = 2\pi\frac{\phi_{\text{ext}}}{\phi_0}$, where ϕ_{ext} is the external flux through the loop. After these considerations, the Hamiltonian transforms into

$$\mathcal{H}_{\text{SQ}} = 4E_C n^2 - 2E_J \cos\left(\frac{\varphi_1 + \varphi_2}{2}\right)\cos\left(\frac{\varphi_1 - \varphi_2}{2}\right) = 4E_C n^2 - 2E'_J \cos\varphi, \tag{1.33}$$

where $\varphi = (\varphi_1 + \varphi_2)/2$ and $E'_J = 2E_J \cos(\pi\phi_{\text{ext}}/\phi_0)$. Note that the term of the Hamiltonian related to the inductances is equivalent to the potential energy of a single Josephson element with a tunable Josephson energy (E'_J). This is modified by controlling the threading external flux with a magnetic field. Therefore, the Hamiltonian is a periodical function in ϕ_{ext}, with a period of $2\phi_0$. In the case of $E_{J1} \neq E_{J2}$ the result is slightly more complex, but the behaviour of the Hamiltonian is similar [4].

1.2.4 Josephson Junction Array

A set of Josephson junctions in series present a particular characteristic that make it a very useful device in superconducting circuits. Let us consider M identical Josephson junctions and suppose that the capacitances across them can be neglected. This allows the reduced flux across the array φ to be equally distributed among all the junctions [4]. The Hamiltonian of a JJ array results in

$$\mathcal{H}_{\text{arr}} = -ME_J \cos(\varphi/M). \tag{1.34}$$

This expression is only valid when the electrostatic energy, $E_C = e^2/2C_\Sigma$, is much smaller than E_J. For large values of M the argument of the cosine is very small, so we can approximate the Hamiltonian to its second-order expansion,

$$\mathcal{H}_{\text{arr}} \approx -\frac{E_J}{2M}\varphi^2. \tag{1.35}$$

Comparing this result with Eq. 1.8 we notice that an array of JJ can be considered as a linear inductance with $\mathcal{L}_{\text{arr}} = M/E_J$ under certain conditions. This is known as a superinductance due to the large value of $\mathcal{L}_{\text{arr}}$, which is not obtainable with geometric inductances [4].

Chapter 2

Superconducting Qubits

A qubit is the basic unit of information in quantum computing, analogous to the bit in classical computing. Physically, it is a two-level quantum system. There exist two different kind of qubits in quantum platforms. The first type takes advantage of finite-dimensional quantum systems which already exist in nature, such as the spin of an electron or the polarization of a photon. The second one, however, makes use of anharmonic infinite-dimensional systems which are non-linear, so that we are able to address the transition between only two levels. A paradigmatic example of the latter group is the superconducting qubit, in which the Josephson junction plays a crucial role, as explained in Section 1.2.2.

In this Chapter, we present the three simplest superconducting qubits which contain only one Josephson junction. These are the charge qubit (Cooper pair box), the flux qubit (RF SQUID) and the phase qubit (current-biased Josephson junction). In Section 2.4, we introduce the circuit quantum electrodynamics (cQED) [7]. This research field studies the interaction between a superconducting qubit and a waveguide resonator, which can be considered analogous to the interaction between electromagnetic radiation and an atom in a cavity. Finally, in Section 2.5, we briefly comment some experimental aspects about superconducting circuits, such as the materials and the ranges of temperatures and operational frequencies. To conclude, we present a real picture of a superconducting circuit for cQED obtained from Ref. [8] identifying the different components observed in the picture.

2.1 Charge Qubit

The charge qubit, also known as Cooper pair box, is a superconducting qubit made of a Josephson junction shunted by a linear capacitance, so that $E_J/E_C \ll 1$ (small Josephson junction), and controlled by a voltage source. This circuit can be understood as a superconducting island connected to a reservoir of charge through a Josephson junction (see Fig. 2.1a). The

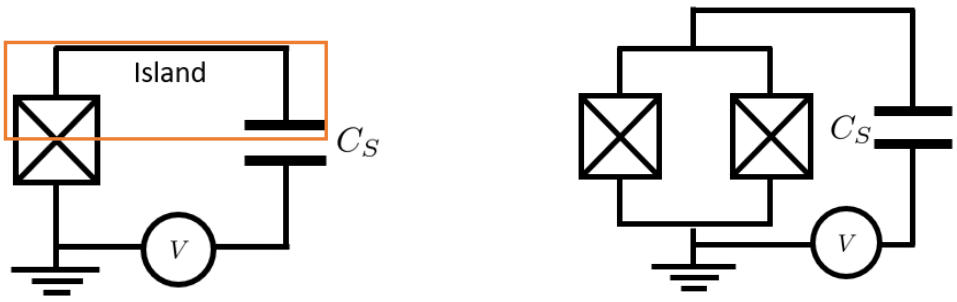

(a) (b)

Figure 2.1: **(a) Cooper Pair Box and (b) Split Cooper Pair box.** The island, in an orange box, is connected to a reservoir (ground) through the Josephson junction (a) or through a DC SQUID (b) with inductance L_J and capacitance C_J. The junction is biased by a controllable voltage source V in series with a linear capacitance C_S.

Hamiltonian of the circuit is

$$\mathcal{H} = 4E_C(n - n_S)^2 - E_J \cos(\varphi). \tag{2.1}$$

Notice that there is only one thing that distinguishes this Hamiltonian from Eq. 1.31, which is the term $n_S = \frac{VC_S}{2e} + Q_o$, where V is the voltage of the source, C_S is the shunting capacitance and Q_o is the possible offset charge on the island. This parameter is externally controllable, since it is proportional to the applied voltage, which allows us to tune the Hamiltonian [6], usually with an external electric field. As the electrostatic energy (E_C) is the dominant term, the state of the circuit is determined by the number of charges n (Cooper pairs) which have tunnelled across the junction into the island. For this reason, the circuit is also known as charge qubit.

By replacing the JJ of a Cooper pair box (Fig. 2.1a) by two of them in parallel (DC SQUID) we can modify the energy levels of the qubit via an external magnetic field. The resulting qubit is known as split Cooper pair box (Fig. 2.1b).

2.2 Flux Qubit

The flux qubit has its origin in the RF SQUID, which is a Josephson junction shunted by an inductance creating a loop, in which an external flux ϕ_{ext} is applied (see Fig. 2.2a). However, flux qubit also refers sometimes to a Josephson junction shunted by a Josephson junction array instead of a geometric inductance. Its Hamiltonian can be approximated by the Hamiltonian of a linear inductance, as we have shown in Eq. 1.35. The Hamiltonian of a RF SQUID results in

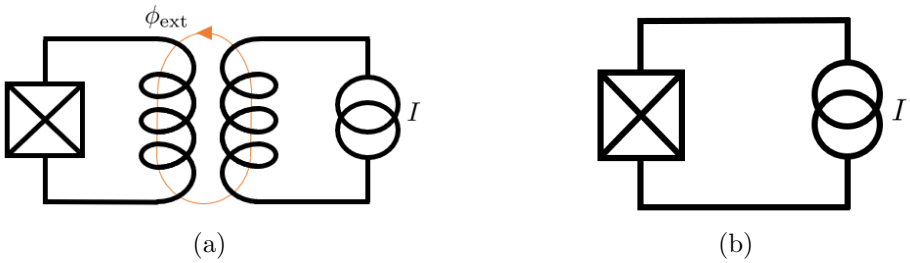

(a) (b)

Figure 2.2: **(a) RF SQUID (flux qubit) and (b) current biased Josephson junction (phase qubit).** with inductance L_J and capacitance C_J.

$$\begin{aligned}\mathcal{H} &= \frac{C_J}{2}\dot{\phi}^2 + \frac{1}{2L}\phi^2 - E_J \cos\left[\frac{2e}{\hbar}(\phi - \phi_{\text{ext}})\right] \\ &= 4E_{CJ}n^2 + \frac{1}{2}E_L\varphi^2 - E_J\cos(\varphi - \varphi_{\text{ext}}),\end{aligned} \tag{2.2}$$

where the electrostatic energy E_{CJ} corresponds to the capacitance of the Josephson element and ϕ_{ext} is the external flux throughout the loop. As there is no longer an isolated island, this circuit is insensitive to any offset charge Q_o [6]. In order to reduce the effects of possible fluctuations in the charge, the regime $E_J/E_{CJ} \ll 1$ is chosen, so the term related to the charge is not dominant in the Hamiltonian. The eigenstates of the flux qubit are states of current in the loop (clockwise or anticlockwise), and the excitation energy of the ground state is a function of E_J and ϕ_{ext}, and therefore, controllable by an external applied flux.

2.3 Phase Qubit

The phase qubit (Fig. 2.2b) consists of a large Josephson junction ($E_J/E_C \gg 1$) biased by a DC current I. We can consider that the current is generated by a inductance with $L \to \infty$ crossed by a flux $\phi \to \infty$, so that $I = \phi/L$. The Hamiltonian describing the dynamics of this circuit is

$$\begin{aligned}\mathcal{H} &= 4E_{CJ}n^2 - \frac{1}{2\pi}I\phi_0\varphi - E_J\cos(\varphi) \\ &= 4E_{CJ}n^2 - I\varphi_0\varphi - I_C\varphi_0\cos(\varphi) \\ &= 4E_{CJ}n^2 - E_J\left(\frac{I}{I_C}\varphi + \cos(\varphi)\right),\end{aligned} \tag{2.3}$$

where I is the applied current, I_C is the critical current of the Josephson junction and $\varphi_0 = \phi_0/2\pi$. The potential in φ has the shape of a tilted dashboard, as we will see in the following Chapter. As well as the flux

qubit, the phase qubit is not affected by charge offset Q_o, and E_J/E_C is chosen large for the same reason as for the flux qubit.

Using Eq. 1.29, we can find the frequency of the classical oscillation in the minima of a well, also known as plasma frequency, which leads to [6]

$$\omega_p = \frac{1}{\sqrt{L_J(I)C_J}} = \sqrt{\frac{I_C\cos(\varphi)}{\varphi_0 C_J}} \approx \frac{1}{\sqrt{L_{J0}C_J}}\left(1-(I/I_C)^2\right)^{1/4}, \qquad (2.4)$$

where $L_J(0) = \varphi_0/I_C$. Considering the circuit as a quantum system, the levels in the well are not equally spaced, and the transition frequency of the two lowest states is $\omega_{01} \approx 0.95\omega_p$, therefore, tunable by changing the value of the bias current I.

2.4 Circuit QED

The interaction between a single-mode of a cavity and a two-level system is described by the Jaynes-Cummings model [9]. We consider that the qubit is much smaller than the resonator, so it can be considered a point. This is known as dipole approximation. The Hamiltonian of the system, known as the quantum Rabi Hamiltonian, is

$$\mathcal{H} = \frac{\hbar\omega_q}{2}\sigma_z + \hbar\omega_f a^\dagger a + \hbar g\sigma_x(a^\dagger + a), \qquad (2.5)$$

where $\hbar\omega_q$ denotes the excitation energy of the qubit, ω_f the frequency of the field in the cavity and g the strength of the interaction. The qubit operators are denoted by Pauli matrices σ_x and σ_z, whereas the ladder operators a, $a^\dagger$ refer to the field in the cavity. If the coupling is small in comparison to the resonator frequency ($g \ll \omega_f$), the quantum Rabi Hamiltonian can be simplified by the rotating wave approximation. This results in the so-called James-Cumming Hamiltonian [10],

$$\mathcal{H}_{\text{RWA}} = \frac{\hbar\omega_q}{2}\sigma_z + \hbar\omega_f a^\dagger a + \hbar g(\sigma_- a^\dagger + \sigma_+ a), \qquad (2.6)$$

where $\sigma_\pm = (\sigma_x \pm i\sigma_y)/2$ are the ladder operators for the qubit, so that $\sigma_+|0\rangle = |1\rangle$ and $\sigma_-|1\rangle = |0\rangle$ ($\sigma_+|1\rangle = \sigma_-|0\rangle = 0$).

The system operates in different regimes depending on the relation between the parameters of the Hamiltonian g, ω_f and ω_q. In the so-called dispersive limit the coupling strength is much smaller than the detuning between the resonator and the qubit, $g \ll |\omega_q - \omega_f|$. In this regime, the qubit readout can be performed by applying a microwave signal to the resonator and measuring the reflection properties [10]. Taking into account this approximation [2], the Hamiltonian results in

$$\mathcal{H}_{\text{dis}} = \frac{\hbar\tilde{\omega}_q}{2}\sigma_z + \hbar\tilde{\omega}_f a^\dagger a, \qquad (2.7)$$

where $\tilde{\omega}_f = \omega_f + \chi\sigma_z$, $\chi = g^2/|\omega_q - \omega_f|$ is the dispersive shift, and $\tilde{\omega}_q = \omega_q + \chi$ is known as Lamb shift. Notice that this Hamiltonian describes a situation in which the qubit and the resonator have no direct interaction, but the resonator suffers a frequency shift which depends on the state of the qubit.

2.4.1 Readout Signal

The capability of measuring the state of the qubit of the system (readout) in a fast and reliable manner is fundamental. We have seen that, in the dispersive limit, the resonator suffers a frequency shift depending on the state of the qubit (χ), a characteristic that can be used for the readout of the state of the two-level system. This is performed by probing the system with a short microwave signal with a frequency ω_R, called carrier frequency, and measuring the reflection properties. The reflected signal is given by

$$s(t) = A_R \cos(\omega_R t + \theta_R), \tag{2.8}$$

where A_R and θ_R are the amplitude and phase of the returning signal. The information about the qubit state is stored in these parameters. This expression can be written as the real part of an exponential,

$$s(t) = \mathrm{Re}\left[A_R e^{i(\omega_R t + \theta_R)}\right] = \mathrm{Re}\left[A_R e^{i\theta_R} e^{i\omega_R t}\right]. \tag{2.9}$$

In this representation, all the information is contained in the phasor $A_R e^{i\theta_R}$. The objective of the readout is to measure the in-phase I and quadrature Q parts of the phasor: $A_R e^{i\theta_R} = I + iQ$.

Let us briefly discuss a method to obtain I and Q called microwave homodyne detection [2] with an I-Q mixer. This procedure consists in comparing the signal which carries the information $s(t)$ against a local signal which resembles the carrier one as if it had no information, i.e. with the same frequency, $y(t) = A_L \cos(\omega_R t)$. Both signals are split into two equal parts, $s(t) = s_I(t) + s_Q(t)$ and $y(t) = y_I(t) + y_Q(t)$. One of the parts of the carrier signal is multiplied by one half of the local one. The other half of the carrier signal is multiplied by the local oscillator shifted a $\pi/2$ phase. The resulting signals are:

$$\begin{aligned} I(t) = s_I(t) y_I(t) &= \frac{A_R}{2}\cos(\omega_R t + \theta_R)\frac{A_L}{2}\cos(\omega_R t) \\ &= \frac{A_R A_L}{8}(\cos(2\omega_R t + \theta_R) + \cos(\theta_R)), \end{aligned} \tag{2.10}$$

and

$$\begin{aligned} Q(t) = s_Q(t) y_Q(t) &= -\frac{A_R}{2}\cos(\omega_R t + \theta_R)\frac{A_L}{2}\sin(\omega_R t) \\ &= \frac{A_R A_L}{8}(\sin(2\omega_R t + \theta_R) - \sin(\theta_R)). \end{aligned} \tag{2.11}$$

Notice that both $I(t)$ and $Q(t)$ contain two different terms, namely, an AC term with a frequency twice the sent signal and a DC term. A low-pass filter is employed in order to take only the DC contributions,

$$I = \frac{A_R A_L}{8}\cos(\theta_R)\,, \qquad Q = \frac{A_R A_L}{8}\sin(\theta_R) \tag{2.12}$$

from which we can obtain the desired amplitude $A_R = 8\sqrt{I^2+Q^2}/A_L$ and phase $\theta_R = \arctan(Q/I)$.

2.5 Experimental Aspects

Until this point, we have discussed the theoretical bases of the different building blocks of a superconducting circuit. However, the technical specifications and the experimental aspects are equally important. In this Section, we briefly introduce different topics related with the experimental realization of a integrated superconducting circuit [6].

2.5.1 Temperature and Frequency Ranges

There are mainly two requirements for an integrated circuit to show a quantum behaviour, namely, low energy dissipation and low noise in the system.

In order to carry a signal from one part of the circuit to another without energy loss, a material with no electrical resistance is necessary, superconductors. Typical choices for this task are low temperature superconductors, such as aluminium or niobium [6].

However, employing superconductors is not a sufficient condition to preserve the quantum states of the circuit. We also need low thermal noise, which is related with the temperature of the system. We must cool it down so that the thermal energy $k_B T$ is much smaller than the energy required to excite a qubit, $k_B T \ll \hbar\omega_{01}$.

The working temperature of superconducting circuits is mainly determined by the Bose-Einstein distribution, which gives an estimation of the number of photons with frequency between ν and $\nu + d\nu$ per unit volume at a given temperature T:

$$n(\nu) \approx \frac{1}{e^{\frac{h\nu}{k_B T}} + 1}, \tag{2.13}$$

where k_B is the Boltzmann constant. If we consider a working frequency of 5 GHz and a temperature of 298 K, the number of photons with the same frequency due to the temperature are $n \approx 1240$. Reducing the temperature to 1 K would result in $3-4$ thermal noise photons, which are still too many if we want to work with single photons. Indeed, the superconducting qubits operate in the microwave regime with frequencies between 3-5 GHz, and the

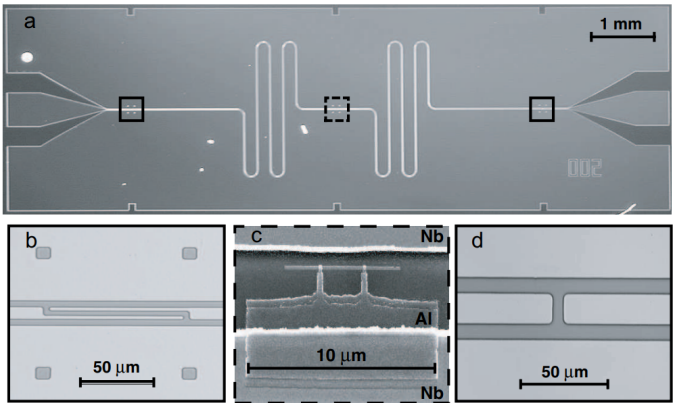

Figure 2.3: **Real picture of a superconducting circuit [8].** (a) Coplanar waveguide resonator fabricated employing optical lithography. (b) Coupling capacitance formed by two fingers. (c) Scanning electron picture of a Cooper pair box located in the center of the resonator. (b) Simple coupling capacitance.

temperature T is around $10 - 30$ mK, which translates into less than 10^{-4} microwave thermal photons per unit volume.

We have to keep in mind that the metals must lie below a certain temperature, called the critical temperature T_c, to present superconducting properties. This temperature is $T_c = 1.2$ K for the aluminium and $T_c = 9.26$ K for the niobium. Due to the requirement of low noise, this condition is already fulfilled for both elements. The higher critical temperature of the niobium makes it a better option than aluminium in terms of feasibility, but the aluminium is much more abundant and cheap.

2.5.2 Fabrication and Design

The techniques of fabrication of superconducting circuits are similar to the ones used for classical integrated circuits. These are the photolithography or e-beam lithography on silicon (Si) or sapphire (Al_2O_3) wafers and the posterior thin-film deposition of the metal [6].

In order to consider that the elements of our circuit are ideal, their dimension must be much smaller than the wavelength of the signal operating in our circuit. This is known as the lumped element approximation, and it forces the size of the elements to be much smaller than the typical wavelength of the signal, which is around 1 cm.

2.5.3 Example of a Superconducting Circuit

Let us now characterize the real superconducting circuit depicted in Fig. 2.3, which is taken from Ref. [8]. This chip comprises a transmission line resonator and a superconducting qubit. The resonator is made of a niobium coplanar waveguide fabricated employing photolithography. The width of

the centre line is 10 μm and it forms a gap with the ground planes of 5 μm. Since the length of the transmission line (2.4 cm) is greater than the size of the chip, it must be displayed in a sinusoidal form.

The output and input ports are connected to the resonator by two capacitors of different architectures but identical values. The left one (b) is made of two superconducting fingers, 4 μm wide and 100 μm long, separated by a 2 μm gap. The right coupling capacitance (d) is made with a gap of 4 μm.

The final component (c) is a split Cooper pair box, introduced in Section 2.1, made of aluminium employing electron beam lithography. It is situated between the central line and the bottom ground plane of the coplanar waveguide. The ground plane is connected to the island through the SQUID, and the island forms a capacitance with the central line of the resonator.

Chapter 3

Photodetector Proposal

Single flying photon photodetectors are a essential tool in quantum optics, required for almost every quantum protocol involving photons. This device already exists for the optical regime, which is commercially available. This is the case of the single-photon avalanche diode (SPAD) [11]. It is a single-photon detector based on the avalanche current triggered when radiation is applied to a reverse biased p-n junction. A single optical photon unleashes a charge carrier which, thanks to a high electric field, is capable of triggering an avalanche of electrons. However, due to the low energy of microwave photons (≈ 0.1 meV) in comparison to the energy of optical photons (≈ 1 eV), we cannot take advantage of this effect to design a single-photon detector for microwaves.

In this Chapter, we describe the proposal of a 100% efficient single-photon detector in the microwave regime introduced in Ref. [12]. This perfect photodetector relies on the interaction between the photon on a semi-infinite transmission line and a mirror at the end with a phase qubit at a fixed distance L from the mirror. Firstly, in Section 3.1 we explain the motivation for using the current-biased Josephson junction, briefly reviewed in Section 2.3 (see Fig. 2.2b). We also develop the basic tools for the analysis of any photodetector based on an interaction between a transmission line and a qubit with a washboard potential.

In Section 3.2, we present the setup of the microwave detector proposal, consisting of a semi-infinite line and a qubit placed at a given distance from a perfect mirror, which is at the end of the transmission line. We analyse its performance and calculate the efficiency for one single qubit (absorber). Finally, the analysis is generalized for the case of N absorbers.

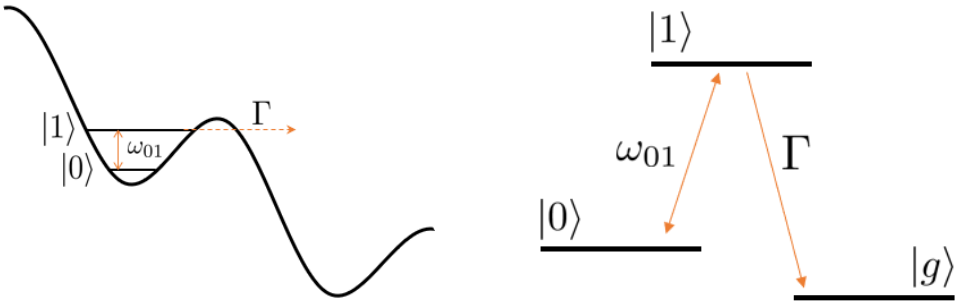

(a) (b)

Figure 3.1: **(a) Tilted dashboard potential of Eq. 2.3 and (b) three level Λ system representation.** The energy needed to excite the state $|0\rangle$ is given by $\hbar\omega_{01}$, and the state $|1\rangle$ decays to a continuum with a rate Γ.

3.1 Photodetection with Current-Biased Josephson Junctions

The most important feature of a current-biased Josephson junction (CBJJ) or any other phase qubit is its built-in readout, which is due to the shape of its potential (Fig. 3.1a). The readout of a phase qubit is possible thanks to a quantum effect known as quantum tunnelling, a phenomenon which allows a particle to tunnel through a potential barrier. This effect allows a photon in the state $|1\rangle$ to cross the barrier into the continuum with a rate Γ, generating a voltage difference across the Josephson junction [6]. The tunnelling rate of the state $|0\rangle$ is approximately 500 times smaller than the one for the state $|1\rangle$ and, therefore, can be neglected. This is known as a three-level Λ system, which is represented by the scheme in Fig. 3.1b.

The performance of a photodetector is given by the probability of absorbing an arriving photon. In order to calculate it, we need the Hamiltonian of the system, which is

$$\mathcal{H} = \hbar(\omega_{01} + i\Gamma/2)\,|1\rangle\langle 1| + i\hbar v_g \int dx(\psi_L^\dagger \partial_x \psi_L - \psi_R^\dagger \partial_x \psi_R)$$
$$+ \hbar V \int dx\delta(x - x_i)[(\psi_R + \psi_L)\,|1\rangle\langle 0| + H.c.]. \tag{3.1}$$

The first term of the non-Hermitian Hamiltonian corresponds to the Λ system, where $\hbar\omega_{01}$ is the excitation energy of the qubit and Γ is the decay rate of the state $|1\rangle$ to the continuum $|g\rangle$. This term can be understood in the following way: the evolution of a wave function $\Phi(x, t = 0)$ is given by $\Phi(x,t) = e^{-i\mathcal{H}t/\hbar}\Phi(x,0)$, where $\mathcal{H}$ is the Hamiltonian of the system. The decay of a function is given by $\Phi(x,t)e^{-\Gamma t}$, where Γ is the decay rate. Therefore, the evolution of a decaying function is $\Phi(x,t)e^{-i(-i\hbar\Gamma)t/\hbar}$, where $-i\hbar\Gamma$ can be considered the Hamiltonian term responsible for the decay.

The second term is associated to the propagating electromagnetic fields, where $\psi_{R/L}$ is the wave function of the field travelling right/left. The energy of a radiation field is the expected value $\hbar\omega_p h = \hbar v_g k = v_g p$, with v_g the group velocity of the propagating photon and p the momentum operator, which is defined as $-i\hbar\partial_x$.

The third and last term corresponds to the interaction between the photon and the qubit, where H.c. denotes the Hermitian conjugate. It is modelled with a delta potential $V\delta(x)$ located at the position of the qubit x_i, and is the responsible for exciting the qubit from the state $|0\rangle$ to $|1\rangle$. This Hamiltonian generates the evolution of the quantum state of the system which, in the case of a state with zero or one photons, leads to

$$|\phi\rangle = \int dx[\xi_R(x,t)\psi_R^\dagger(x) + \xi_L(x,t)\psi_L^\dagger(x)]\,|0,\mathrm{vac}\rangle + e(t)\,|1,\mathrm{vac}\rangle\,, \tag{3.2}$$

where $|0,\mathrm{vac}\rangle$ is the state of the system with the absorber in the state 0 and the field in vacuum. The operator $\psi_{R/L}^\dagger(x)$ applied to the state $|vac\rangle$ creates a photon moving to the right/left at the position x. The function $\xi_{R/L}$ represents the wave-packet of a single photon moving to the right/left. Finally, the function $e(t)$ denotes the population of the excited state of the absorber.

Let us now find the efficiency of the design, which is defined as the probability of finding the system the state $|g\rangle$ at long times. This would mean that the absorber has detected a photon. The probability is calculated as $P_g = 1 - ||\phi||^2$ [1], where $||\phi||^2$ is the probability of finding the system in any other state. For this, we need to find the value for the coefficients $\xi_{R/L}$ and $e(t)$, which is done by solving the Schrödinger equation $i\hbar\frac{\partial}{\partial t}|\phi\rangle = \mathcal{H}|\phi\rangle$, for the state given by Eq. 3.2 with the Hamiltonian provided in Eq. 3.1. This results in the three following equations, which relate the field amplitudes $\xi_{R/L}$ with the absorber population $e(t)$:

$$\begin{aligned} i\partial_t\xi_R(x,t) &= -iv_g\partial_x\xi_R(x,t) + V\delta(x)e(t), \\ i\partial_t\xi_L(x,t) &= +iv_g\partial_x\xi_L(x,t) + V\delta(x)e(t), \\ (i\partial_t - \omega_{01} + i\Gamma/2)e(t) &= V/2[\xi_R^+(t) + \xi_R^-(t) + \xi_L^+(t) + \xi_L^-(t)], \end{aligned} \tag{3.3}$$

where we have considered that the absorber is located in the origin ($x_i = 0$) and $\xi_{R/L}^\pm(t) = \xi_{R/L}(0^\pm, t)$ are the wavepackets just before $(-)$ and after $(+)$ the absorber (see Fig. 3.2a).

Integrating the first two equations, the conditions for the field around the absorber hold

$$\xi_R^+(t) = \xi_R^-(t) - i\frac{V}{v_g}e(t)\,, \qquad \xi_L^-(t) = \xi_L^+(t) - i\frac{V}{v_g}e(t). \tag{3.4}$$

We can now replace this boundary conditions into the third Eq. 3.3, which

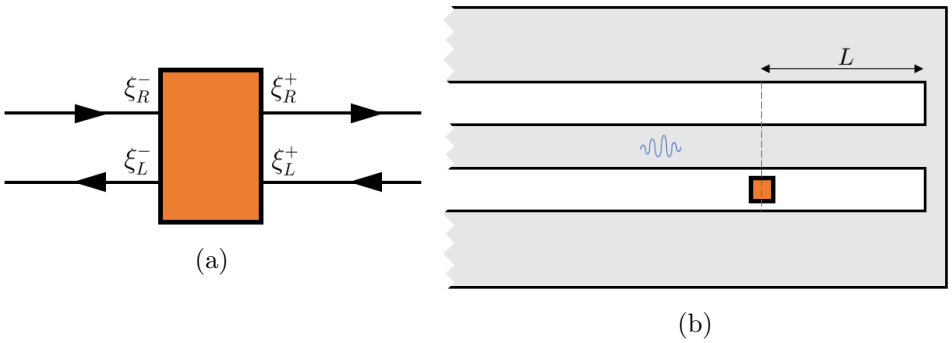

Figure 3.2: **(a) Scheme of the absorber and the fields around it propagating to the right (R) or left (L). (b) Representation of the complete system proposed in Ref. [12].** The absorber is represented by an orange square, and it is located in a transmission line separated a distance L from the mirror at the end of the transmission line.

leads to an ordinary differential equation for the population $e(t)$ of the excited state,

$$i\partial_t e(t) - \left[\omega_{01} - i(\Gamma/2 + V^2/v_g)\right] e(t) - V(\xi_R^- + \xi_L^+) = 0. \tag{3.5}$$

Notice that the decaying term, which was previously $i\Gamma/2$, has been amplified by the interaction of the Λ system with the transmission line by iV^2/v_g, where V is the strength of the interaction and v_g is the group velocity.

3.2 Photodetector with a Mirror

The analysis performed in the previous Section is common for every design consisting of a Λ system interacting with a transmission line. The remaining terms are the entering fields to the absorber from the left (ξ_R^-) and from the right (ξ_L^+). These terms depend on the specific design of the photodetector. For instance, in the case of an absorber in an infinite transmission line, we would only expect an entering field from one of the sides, for example, from the left $\xi_R^- = \Phi(t)$, which implies $\xi_L^+ = 0$. After interacting with the absorber, one part is transmitted (ξ_R^+) and another part is reflected (ξ_L^-).

3.2.1 Single Absorber

The proposal developed in Ref. [12] comprises a mirror located a distance L from the phase qubit (see Fig. 3.2b). In this case, the transmitted part of $\Phi(t)$ is totally reflected by the mirror with a phase change given by the factor κ. The wave reflected by the mirror enters to the absorber from the left after a certain time a. Therefore, the entering field ξ_L^+ results in

$$\xi_L^+(t) = \kappa\xi_R^+(t-a) = \kappa\Phi(t-a) - i\frac{\kappa V}{v_g}e(t-a), \tag{3.6}$$

where we have employed Eq. 3.4. The time taken by the signal to reflect in the mirror an return to the absorber is $a = 2L/v_g$. We can replace this equation into Eq. 3.5, resulting in a delay differential equation (DDE),

$$i\partial_t e(t) - \left[\omega_{01} - i\left(\frac{\Gamma}{2} + \frac{V^2}{v_g}\right)\right] e(t) - V(\Phi(t) + \kappa\Phi(t-a) - i\frac{\kappa V}{v_g}e(t-a)) = 0. \tag{3.7}$$

Due to the difficult treatment of these equations, an approximation for the wavepacket $\Phi(t)$ is taken for the sake of simplicity. This is the adiabatic modulation, which assumes that the function can be written as

$$\Phi(t) = \chi(t)e^{-i\omega_0 t}, \tag{3.8}$$

where ω_0 is the frequency of the wavepacket and $\chi(t)$ varies slowly with respect to the exponential, $|\partial_t\chi(t)| \ll \omega_0$. Therefore, the function displaced a sufficiently small time a results in

$$\Phi(t-a) = \chi(t)e^{-i\omega_0 t}e^{i\omega_0 a}. \tag{3.9}$$

This assumption implies that the absorber population evolves with the same frequency $e(t) = f(t)e^{-i\omega_0 t}$. Applying these changes to Eq. 3.7, we obtain

$$\begin{aligned} &i\partial_t f(t) + \omega_0 f(t) - \left[\omega_{01} - i\left(\frac{\Gamma}{2} + \frac{V^2}{v_g}\right)\right] f(t) - V(\chi(t) + z\chi(t) - i\frac{zV}{v_g}f(t)) = \\ &i\partial_t f(t) + i\frac{V^2}{v_g}\left[1 + \frac{v_g}{V^2}\left(\frac{\Gamma}{2} + i(\omega_{01} - \omega_0)\right)\right] f(t) - V(1+z)\chi(t) + i\frac{zV^2}{v_g}f(t) \\ &= i\partial_t f(t) + i\frac{V^2}{v_g}(1 + \gamma + z)f(t) - V(1+z)\chi(t) = 0, \end{aligned} \tag{3.10}$$

where $z = \kappa e^{i\omega_0 a}$ and $\gamma = \frac{v_g}{V^2}\left(\frac{\Gamma}{2} + i(\omega_{01} - \omega_0)\right)$. Making the change $f(t) = v_g x(t)/V$ and the change of variable $t = v_g\tau/V$, the previous equation yields

$$\partial_\tau x(\tau) + i(1 + \gamma + z)x(\tau) = -i(1+z)\chi(\tau), \tag{3.11}$$

which is a non-homogeneous linear first-order differential equation. It can be straightforwardly solved for $x(\tau)$,

$$x(\tau) = -i(1+z)\int_{-\infty}^{\tau} e^{-(1+\gamma+z)(\tau-s)}\chi(s)ds. \tag{3.12}$$

To sum up, we have found $x(\tau)$ and, therefore, the population of the excited state of the qubit $e(t)$, in terms of two free parameters z and γ, as well as of the exact form of the wavepacket $\chi(t) \to \phi(t)$.

In order to finally calculate $e(t)$ and, consequently, the efficiency of the photodetector, we need to choose the shape of the wavepacket. In this work, the performance is analysed with a normalized Gaussian wavepacket,

$$\chi(\tau) = \frac{1}{\sqrt{\sigma\pi^{1/2}}}e^{-\tau^2/(2\sigma^2)}, \tag{3.13}$$

where σ is the variance. This function only makes sense if it varies slowly with respect to ω_0 ($|\partial_t \chi(t)| \ll \omega_0$), this is, $\sigma \gg \omega_0^{-1}$.

We have now all the ingredients for computing the efficiency of this proposal, which is the probability of absorbing the photon and tunnelling to the state $|g\rangle$. For long times, the probability of the decay of the state $|1\rangle$ is 1, thus we can define the efficiency of the detector as the fraction of the signal, the wavepacket, that was absorbed, i.e. one minus the fraction of the outgoing wavepacket (ξ_L^-) over the incoming one (ξ_R^-),

$$\alpha = 1 - \frac{\int_{-\infty}^{\infty} \left|\xi_L^-(t)\right|^2 dt}{\int_{-\infty}^{\infty} \left|\xi_R^-(t)\right|^2 dt} \tag{3.14}$$

As the Gaussian wavepacket is normalized, the denominator results in

$$\int_{-\infty}^{\infty} \left|\xi_R^-(\tau)\right|^2 d\tau = \int_{-\infty}^{\infty} \left|\chi(\tau) e^{-i\omega_0' \tau}\right|^2 d\tau = \int_{-\infty}^{\infty} \chi(\tau)^2 d\tau = 1. \tag{3.15}$$

The numerator is obtained from Eqs. 3.4 and 3.6, which yields

$$\begin{aligned}
&\int_{-\infty}^{\infty} \left|\xi_L^-(\tau)\right|^2 d\tau = \int_{-\infty}^{\infty} \left|\xi_L^+(\tau) - i\frac{V}{v_g} e(\tau)\right|^2 d\tau \\
&= \int_{-\infty}^{\infty} \left|z\chi(\tau) - (1+z)^2 \int_{-\infty}^{\tau} e^{-(1+\gamma+z)(\tau-s)} \chi(s) ds\right|^2 d\tau \\
&= \int_{-\infty}^{\infty} \frac{e^{-\tau^2/\sigma^2}}{\sigma\sqrt{\pi}} \left|z - \frac{(1+z)^2}{1+z+\gamma}\right|^2 d\tau = \left|z - \frac{(1+z)^2}{1+z+\gamma}\right|^2,
\end{aligned} \tag{3.16}$$

It is useful to write the parameter γ as $\gamma = \Gamma' + i\delta'$, where Γ' is the decay rate and δ' is the detuning between the detector and the photon, $\omega_{01} - \omega_0$, both in units of V^2/v_g. Finally, the expression for the photodetector efficiency α is

$$\alpha = 1 - \left|z - \frac{(1+z)^2}{1+z+\Gamma'+i\delta'}\right|^2 = 1 - \left|-e^{i\theta} - \frac{(1-e^{i\theta})^2}{1-e^{i\theta}+\Gamma'+i\delta'}\right|^2, \tag{3.17}$$

where we have assumed $\kappa = -1$. Notice that the efficiency does not depend on the shape of the Gaussian wavepacket σ, as long as the condition for the adiabatic approximation is fulfilled, $\sigma \gg \omega_0^{-1}$.

In Fig. 3.3, we represent the efficiency of the detector in terms of the decay rate Γ' and the phase change generated by the distance between the mirror and the absorber, θ. The first representation, Fig. 3.3a, corresponds to the case of no detuning between the signal and absorber, $\delta' = 0$. We observe that the detection reaches to a 100% efficiency for $\Gamma' = 2$ and $\theta = \pi$.

Let us now analyse the case in which the photon and the absorber are not in resonance, $\delta' \neq 0$. In Fig. 3.3b, for a value of $\delta' = 0.5$, there are

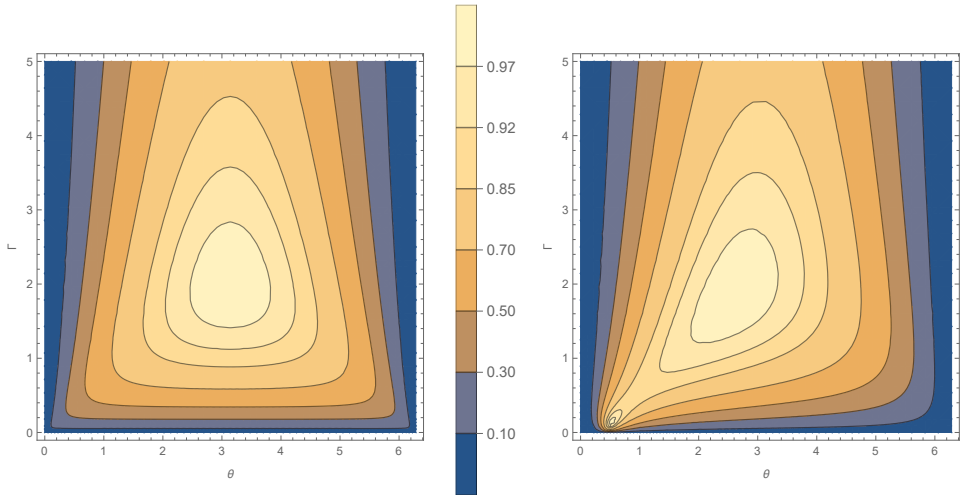

Figure 3.3: **Contour plot of the efficiency in terms of the phase θ and the decay rate Γ'.** (a) No detuned system ($\boldsymbol{\delta' = 0}$). A perfect performance is achieved for $\Gamma' = 2$ and $\theta = \pi$. (b) Slightly detuned system ($\boldsymbol{\delta' = 0.5}$). A perfect performance is achieved for two sets of parameters.

two sets of parameters for which the efficiency reaches 100%. These two points of maximum efficiency come closer as δ' increases, until they become a single point and disappear. This can be seen in Fig. 3.4, where we have plotted the maximum efficiency of the device in terms of the detuning δ'. In this Figure, we can appreciate that an optimal efficiency is achieved until a detuning value of $\delta' \approx 1 \rightarrow \delta = \omega_{01} - \omega_0 \approx V^2/v_g$. Therefore, replacing the values for the parameters V^2/v_g used in Ref. [1], the bandwidth of the detector is $BW \approx 2V^2/v_g \approx 100$ MHz.

3.2.2 Multiple Absorbers

The performance of the detector can be improved by enhancing the operational bandwidth of the device. This is achieved by placing multiple absorbers in the semi-infinite transmission line. In order to find the performance of a multiple absorber photodetector, firstly, we simplify the model by using a monochromatic plane wave $\Phi(t) = e^{(-i\omega_0+\sigma)t}$ instead of a Gaussian wavepacket. Secondly, we introduce an alternative and simpler analysis method [1] that scales with multiple absorbers better than the previous method.

This new method studies the interaction as a scattering process. The first interaction between the signal and the absorber results in reflected and transmitted signals. In this moment, we can consider that the incoming field

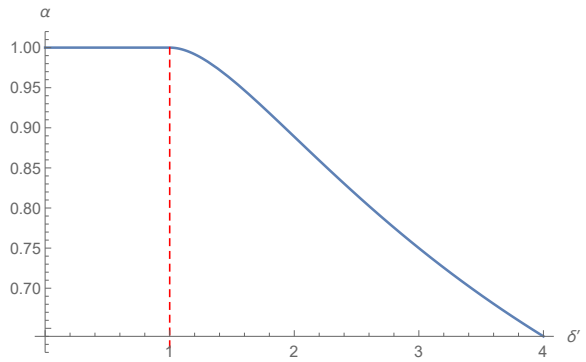

Figure 3.4: **Maximum absorption efficiency α in terms of the detuning δ' .** The red dashed line indicates the maximum detuning for 100% efficiency, which is $\gamma' \approx 1$ in units of V^2/v_g.

by the right is $\xi_L^+ = 0$. Under this assumption, Eq. 3.5 results in

$$i\partial_t e(t) - \left[\omega_{01} - i(\Gamma/2 + V^2/v_g)\right] e(t) - V\Phi(t) = 0. \tag{3.18}$$

The solution of this differential equation is straightforward,

$$\begin{aligned} e(t) &= -iV \int_{-\infty}^{t} e^{-\frac{V^2}{v_g}(1+\gamma)(t-s)+i(\omega_{01}-\omega_0)s} ds \\ &= -i\frac{v_g}{V}\frac{1}{1+\gamma} e^{-i\omega_0 t}. \end{aligned} \tag{3.19}$$

We can find a relation between the population of the excited state and the fields around the absorber by replacing Eq. 3.19 into the third equation of Eqs. 3.3 and solving for $e(t)$, which results in

$$e(t) = \frac{v_g}{iV\gamma}[\xi_R^+(t) + \xi_R^-(t) + \xi_L^+(t) + \xi_L^-(t)] \tag{3.20}$$

Finally, we find the relation between the incoming and outgoing fields by replacing the obtain result into the conditions of Eq. 3.4, which can be written in matrix form as

$$\begin{pmatrix} \xi_R^+ \\ \xi_L^+ \end{pmatrix} = T \begin{pmatrix} \xi_R^- \\ \xi_L^- \end{pmatrix}, \qquad T = \begin{pmatrix} 1 - 1/\gamma & -1/\gamma \\ 1/\gamma & 1 + 1/\gamma \end{pmatrix}, \tag{3.21}$$

where T is the transfer matrix of a single absorber. In the case of N absorbers with a separation between them of L_j, the global transfer matrix is

$$T = \prod_j^N e^{i\frac{2\pi L_j}{\lambda}\sigma_z} \begin{pmatrix} 1 - 1/\gamma_j & -1/\gamma_j \\ 1/\gamma_j & 1 + 1/\gamma_j \end{pmatrix}. \tag{3.22}$$

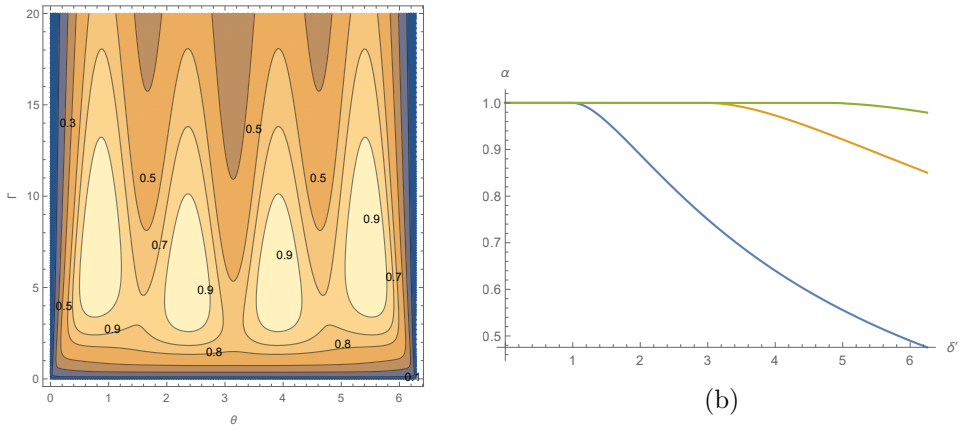

(a) (b)

Figure 3.5: **(a) Contour plot of the efficiency of a 4 absorber resonant detector ($\delta' = 0$)** in terms of the phase θ and the decay rate Γ'. **(b) Maximum efficiency α for $N = 1$ (blue), $N = 4$ (orange) and $N = 8$ (green) absorbers.**

For the sake of simplicity, we will consider that all the absorbers are identical, $\gamma_j = \gamma \; \forall j$, and separated by a constant distance so that $e^{i\frac{2\pi L_j}{\lambda}} = e^{i\theta/2}$. The transfer matrix for N identical equidistant absorbers is

$$T = \left[e^{i\frac{\theta}{2}\sigma_z} \begin{pmatrix} 1 - 1/\gamma & -1/\gamma \\ 1/\gamma & 1 + 1/\gamma \end{pmatrix} \right]^N . \tag{3.23}$$

The particularity of this proposal is the interaction with the mirror, which sets a boundary condition to the field obtained employing Eq. 3.6,

$$\begin{pmatrix} 1 \\ \kappa \end{pmatrix} = e^{i\frac{\theta}{2}\sigma_z} T \begin{pmatrix} \xi_R^- \\ \xi_L^- \end{pmatrix}, \tag{3.24}$$

where $\theta = \omega_0 a$ and κ represents the phase induced by the mirror, typically $\kappa = -1$. Multiplying by $\begin{pmatrix} \kappa\,, & -1 \end{pmatrix}$ both sides of the equation, we obtain an expression for the outgoing field ξ_L^- in terms of ξ_R^-. Making use of this result, we obtain the absorption efficiency from Eq. 3.14, which is given by

$$\alpha = 1 - \left| \frac{T_{11} + e^{-i\theta} T_{21}}{T_{12} + e^{-i\theta} T_{22}} \right|^2 , \tag{3.25}$$

where T_{ij} are the elements of the transfer matrix, which depend on the number of absorbers N, γ and θ. Finally, we find the performance of a detector with four Λ systems, and depict it in Fig. 3.5a in terms of the decay rate Γ' and θ. The detector now offers an optimal efficiency for more sets of parameters, which means that the relative position of the absorbers lacks of importance in the performance. Furthermore, we have also computed and

represented the maximum efficiency in terms of the detuning (Fig. 3.5b) for $N = 1$ (blue), $N = 4$ (orange), and $N = 8$ (green). By observing this figure, we can conclude that increasing N notable enhances the operational bandwidth, for example tripling it in the case of $N = 4$ absorbers.

Chapter 4

Conclusions

We have started this work by describing the main superconducting circuit elements, both linear and non-linear. Then, we have learned how to obtain the Hamiltonian which characterizes the dynamics of superconducting circuits. Finally, we have compared the linear LC oscillator against the Josephson LC circuit. Indeed we have observed that the non-linearity added by the Josephson junction to the LC circuit generates an anharmonic energy spectrum. This feature allows us to address the transition between only two energy levels, which is a fundamental requirement to be employed as a qubit.

Superconducting qubits are key elements in the superconducting circuit platform. We have calculated the Hamiltonian of the simplest ones, namely, the charge, flux and phase qubit, and analysed their fundamental properties. Then, we have reviewed the research field of circuit QED, which studies the interaction between a qubit and a transmission line resonator. We have seen that, in the limit in which the coupling between the qubit and the resonator is small compared with their detuning, it is possible to read the state of the qubit by probing the resonator with a microwave signal and measuring the reflection properties of the system.

The motivation of this work is to study the fundamental models of microwave single-photon photodetectors. We have studied a photodetector based on qubits interacting with a transmission line with a dashboard-like potential and, in particular, we have reviewed the proposal developed in Ref. [12], based on a semi-infinite line with a mirror at the end. We have calculated the efficiency of the photodetector for a single qubit and found that it reaches 100% for some values of the parameters. We have also shown that it operates correctly in a reasonable bandwidth, for which the detection is still perfect. Finally, we have calculated the efficiency of the detector with multiple qubits in the transmission line, and observed that a perfect detection is achieved for a larger set of parameters, which means an improvement in the operational bandwidth and robustness.

An efficient detection of microwave single propagating photons is crucial

in several protocols and technologies, including, for instance, quantum teleportation, quantum sensing and metrology, quantum radars and distributed quantum computing, just to mention a few. The proposal reviewed in this work is a promising candidate for a feasible design of an efficient microwave photodetector, but it is far from being the only one. Only an experimental development and testing will decide which is the optimal approach.

Bibliography

[1] Guillermo Romero, Juan García-Ripoll, and Enrique Solano. Photodetection of propagating quantum microwaves in circuit QED. *Phys. Scr.* **T137**, 014004 (2009).

[2] Philip Krantz, Morten Kjaergaard, Fei Yan, Terry P. Orlando, Simon Gustavsson, and William D. Oliver. A quantum engineer's guide to superconducting qubits. *arXiv:1904.06560* (2019).

[3] Thomas G. McConkey. *Extensible Architecture for Superconducting Quantum Computing.* PhD thesis, University of Waterloo, Canada (2018).

[4] Uri Vool and Michel H. Devoret. Introduction to quantum electromagnetic circuits. *Int. J. Circuit Theory Appl.* **45**, 897 (2017).

[5] Amir. O. Caldeira and Anthony. J. Leggett. Influence of dissipation on quantum tunneling in macroscopic systems. *Phys. Rev. Lett.* **46**, 211 (1981).

[6] Michel H. Devoret and John M. Martinis. In *Experimental Aspects of Quantum Computing*, edited by Henry O. Everitt (Springer US , 2005).

[7] Nathan K. Langford. Circuit QED-lecture notes. *arXiv:1310.1897* (2013).

[8] Luigi Frunzio, Andreas Wallraff, David Schuster, Johannes Majer, and Robert Schoelkopf. Fabrication and characterization of superconducting circuit QED devices for quantum computation. *IEEE Transactions on Applied Superconductivity* **15**, 860 (2005).

[9] Edwin T. Jaynes and Fred W. Cummings. Comparison of quantum and semiclassical radiation theories with application to the beam maser. *Proceedings of the IEEE* **51**, 89 (1963).

[10] David Zueco, Georg Reuther, Sigmund Kohler, and Peter Hanggi. Qubit-oscillator dynamics in the dispersive regime: Analytical theory beyond the rotating-wave approximation. *Phys. Rev. A* **80**, 033846 (2009).

[11] Mario Stipčević, Daqing Wang, and Rupert Ursin. Characterization of a commercially available large area, high detection efficiency single-photon avalanche diode. *Journal of Lightwave Technology* **31**, 23 (2013).

[12] Borja Peropadre, Guillermo Romero, Göran Johansson, Christian M. Wilson, Enrique Solano, and Juan García-Ripoll. Perfect microwave photodetection in circuit QED. *Phys. Rev. A* **84**, 063834 (2010).

Appendices

Appendix A

Mathematica Figures

In this program, we compute the efficiency of the photodetector. Firstly, it is performed for 1 absorber and represented graphically with a contour plot. Then we compute the maximum efficiency for different values of detuning δ'. This is repeated for multiple absorbers, in particular, $N = 4$. Finally we compare the maximum efficiency in terms of δ for $N = 1$, 4 and 8 absorbers.

```
In[ ]:= Gaus[τ_] := 1 / (Sqrt[15 Sqrt[π]]) Exp[-τ^2 / (2 * 15^2)]
        Integrate[Exp[-(1 + γ + z) (τ - s)] Gaus[τ], {s, -∞, τ}]
```

```
Out[ ]= ConditionalExpression[ e^(-τ^2/450) / (√15 π^(1/4) (1 + z + γ)), Re[z + γ] > -1]
```

```
In[ ]:= Res[z_, γ_] := Abs[z - (1 + z)^2 / (1 + z + γ)]
```

Efficiency for 1 absorber:

```
In[ ]:= ContourPlot[1 - Res[-Exp[i θ], Γ]^2, {θ, 0, 2 π},
          {Γ, 0, 5}, Contours → {0.1, 0.3, 0.5, 0.7, 0.85, 0.92, 0.97},
          PlotLegends → Automatic, Frame → True, FrameLabel → Automatic]
        ContourPlot[1 - Res[-Exp[i θ], Γ + i 0.5]^2, {θ, 0, 2 π},
          {Γ, 0, 5}, Contours → {0.1, 0.3, 0.5, 0.7, 0.85, 0.92, 0.97},
          PlotLegends → Automatic, Frame → True, FrameLabel → Automatic]
```

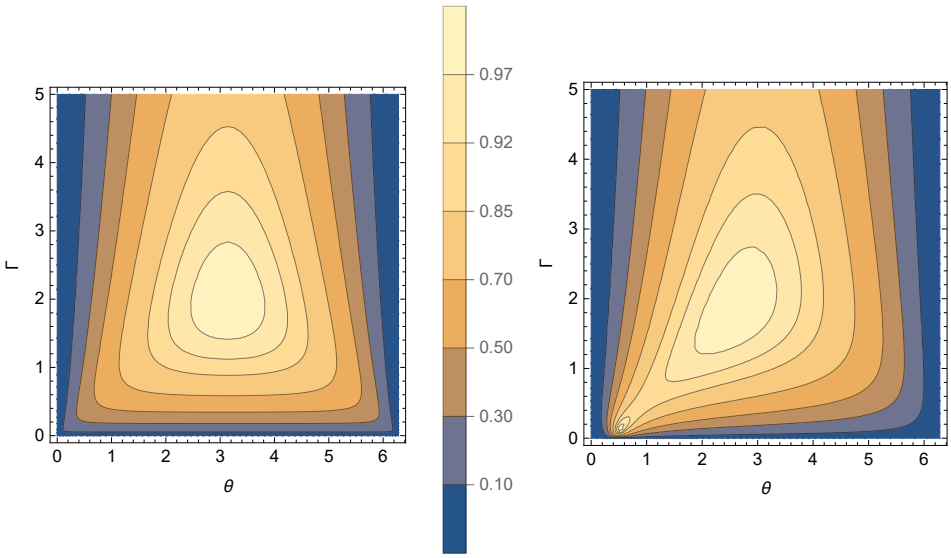

Maximum efficiency in terms of δ:

In[•]:=
```
Plot[{Part[Maximize[1 - Res[-Exp[i θ], Γ + i δ]^2, {θ, Γ}], 1]},
 {δ, 0, 4}, AxesLabel → {δ, α}]
```

Out[•]=

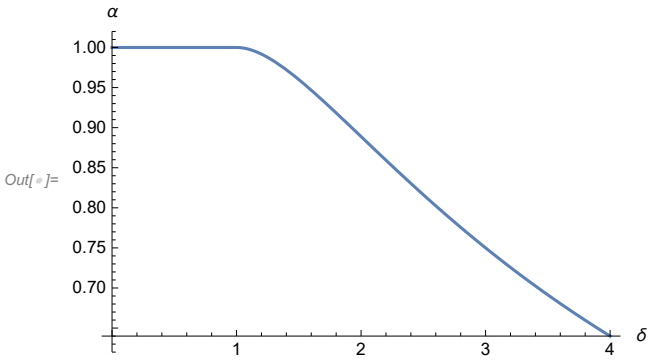

Efficiency for multiple absorbers (N= 4) and maximum efficiency in terms of δ:

In[•]:=
```
Solve[Flatten[{{-1  -1}}.{{Exp[i θ/2], 0}, {0, Exp[-i θ/2]}}.{{T11, T12}, {T21, T22}}.{{eR}, {eL}}] == 0, eL]
```

Out[•]=
$$\left\{\left\{eL \to -\frac{eR\left(e^{i\theta}\,T11 + T21\right)}{e^{i\theta}\,T12 + T22}\right\}\right\}$$

In[•]:=
```
T[γ_] := {{1 - 1/γ, -1/γ}, {1/γ, 1 + 1/γ}}

Ph[θ_] := {{Exp[i θ/2], 0}, {0, Exp[-i θ/2]}}

T1[γ_, θ_] := Ph[θ].T[γ]
T4[γ_, θ_] := T1[γ, θ].T1[γ, θ].T1[γ, θ].T[γ]
T8[γ_, θ_] := T1[γ, θ].T1[γ, θ].T1[γ, θ].T1[γ, θ].T1[γ, θ].T1[γ, θ].T1[γ, θ].T[γ]
```

In[•]:=
```
α1[γ_, θ_] := 1 - Abs[(T[γ][[1, 1]] + e^(-i θ) T[γ][[2, 1]])/(T[γ][[1, 2]] + e^(-i θ) T[γ][[2, 2]])]^2
```
valor absoluto

```
α4[γ_, θ_] := 1 - Abs[(T4[γ, θ][[1, 1]] + e^(-i θ) T4[γ, θ][[2, 1]])/(T4[γ, θ][[1, 2]] + e^(-i θ) T4[γ, θ][[2, 2]])]^2
```
valor absoluto

```
α8[γ_, θ_] := 1 - Abs[(T8[γ, θ][[1, 1]] + e^(-i θ) T8[γ, θ][[2, 1]])/(T8[γ, θ][[1, 2]] + e^(-i θ) T8[γ, θ][[2, 2]])]^2
```
valor absoluto

In[•]:=
```
ContourPlot[α4[Γ, θ], {θ, 0, 2 π}, {Γ, 0, 20}, Contours → {0.1, 0.3, 0.5, 0.7, 0.8, 0.9},
 Frame → True, FrameLabel → Automatic, PlotPoints → 75, ContourLabels → {0.7, 0.8, 0.9}]
```
representación de contornos · contornos · marco · verd··· · etiqueta de ma··· · automático · número de puntos en· · etiquetas de contorno

```
Plot[{Part[NMaximize[α1[Γ + i δ, θ], {θ, Γ}], 1],
  Part[NMaximize[α4[Γ + i δ, θ], {θ, Γ}], 1],
  Part[NMaximize[α8[Γ + i δ, θ], {θ, Γ}], 1]}, {δ, 0, 6.25}, AxesLabel → {δ, α}]
```
repre··· · parte · maximiza aproximadamente

parte · maximiza aproximadamente

parte · maximiza aproximadamente · etiqueta de ejes

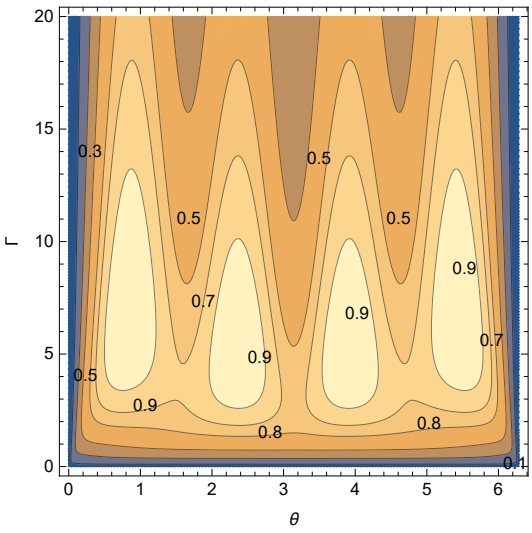
Γ
θ
0.3
0.5
0.5
0.5
0.7
0.9
0.9
0.9
0.7
0.5
0.9
0.8
0.8
0.1

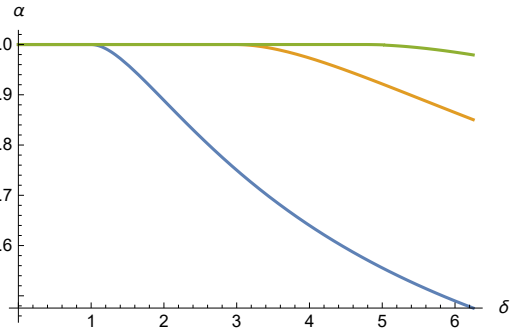
α
δ
1.0
0.9
0.8
0.7
0.6